JOURNAL OF MATERIALS SCIENCE 25 (1990) 5291–5297

The electrical properties of some cordierite glass ceramics in the system $MgO–Al_2O_3–SiO_2–TiO_2$

I. O. OWATE, R. FREER
Materials Science Centre, University of Manchester/UMIST, Grosvenor Street, Manchester, M1 7HS, UK

The a.c. dielectric breakdown and electrical resistivity of glass ceramics in the system $MgO–Al_2O_3–SiO_2–TiO_2$ have been studied using three sets of samples having different crystallinity contents. Standard a.c. (50 Hz) breakdown tests were performed at room temperature (18° C) using planar disc specimens and hemispherically-ended brass contact electrodes. The breakdown process caused the formation of a breakdown channel which terminated at the specimen surface in a crater. The breakdown strength was independent of the rate of voltage rise, but decreased exponentially (60 to 10 $kV\,mm^{-1}$) with increasing specimen thickness. A high crystallinity content, good surface finish and a homogeneous microstructure yielded high breakdown strengths whilst poor microstructural development caused a reduction in breakdown strength. The breakdown mechanism is believed to be a combination of electronic, thermal and electromechanical processes.

1. Introduction

The insulation and dielectric properties of ceramic-based materials (including glass ceramics) are of considerable importance in the fields of electrical engineering and solid state electronics. During the last decade, technological developments have placed increasing demands upon the electrical and structural properties of the insulators [1–4] and revealed the inadequacy of some existing materials [3, 4]. A primary requirement of any candidate material is the ability to withstand high voltages and maintain insulation without suffering serious degradation. If the ceramic or glass–ceramic is to be used as a substrate for the direct mounting of components [5] or simply as a substantial element of solid insulation then mechanical strength is important. For example the utilization of such materials in high voltage instruments or installations, demands the provision of adequate mechanical strength and stability. This dual role means that the mechanical and structural integrity of the insulator is of crucial importance.

The superior electrical and mechanical properties of ceramics, in general, makes them suitable for the more demanding applications in hostile environments of high temperature, high frequency or severe corrosive atmospheres [1, 5]. However, ceramics are brittle in nature and may occasionally break down mechanically or electrically under high stresses. Therefore, high-quality materials and components are essential for systems to be used in the more demanding environments.

Alumina, glass–ceramics and related ceramic-based materials are used extensively in electrical, electronic and structural applications [6–10]. The mechanical properties of most suitable ceramic materials have been investigated in some detail [1, 11], but as yet we have only a limited understanding of the electrical processes occurring in these solid insulators. In particular, the literature suggests that the electrical properties of glass–ceramics have received comparatively little attention [10, 11].

The present study is concerned with the a.c. dielectric breakdown of some cordierite glass–ceramics (in the system $MgO–Al_2O_3–SiO_2–TiO_2$). Glass–ceramics from this family have been used in a variety of applications from radomes to substrates [6, 12] and a.c. conditions are relevant for many. Breakdown tests have been performed in a dedicated test cell/electrode system, which had previously been used for studies of alumina ceramics [13].

Related electrical resistivity and loss factor measurements were also performed in order to try to identify conduction processes and breakdown mechanisms.

2. Materials

2.1. Preparation

The glass–ceramic materials were supplied by Pilkington Brothers Ltd. Three sets of samples were prepared from the same parent glass using different crystallization times and temperatures. The products, hereby classified as GC 138.1, GC 138.2 and GC 138.3 (Table I), were in the form of blocks. These were cut and machined to yield discs of 26 mm diameter and various thicknesses.

2.2. Characterization

The bulk densities of the specimens were determined

0022–2461/90 $03.00 + .12

TABLE I Glass–ceramic specimens

Specimen	Temperature of crystallization (°C)	Time of crystallization (h)
GC 138.1	1300	$\leqslant 5$
GC 138.2	1300	$\leqslant 3$
GC 138.3	1020	$\leqslant 2$

by methods based on Archimedes Principle (following the modified technique defined in ASTM C373) [14]. The results, shown in Table II, are the average of ten individual measurements on each sample.

The specimens for the grain size measurements were prepared in the following way: glass–ceramics from each batch were polished to a mirror-like finish and then etched for 2 min in a hot (400° C) solution of 3:1 by volume of orthophosphoric acid (0.8 N) and nitric acid (0.5 N). Finally, the surface was cleaned by acetate paper soaked in acetic acid, and coated with carbon for scanning electron microscope (SEM) examinations. It is believed that the etchant partly dissolved the silicate (glassy) grain boundary phase thereby revealing the morphology of the grains. Electron micrographs of the surface morphology were obtained for eight different sections on each type of sample. Over 1500 grains (of each type) were examined by an electronic analyser and the planimetric (Jeffries) [15] method. Full details of both techniques are reported elsewhere [16]. Results from the electronic method are summarized in Table II, and the results from the planimetric method are not significantly different.

An X-ray diffraction technique [17–19] was used to determine the fraction of crystallinity in selected specimens. This method is based on the fact that during heat treatment of the parent glass to form the glass–ceramics, crystalline regions are formed at the expense of the glassy phase. It has been established [17, 19] that there is a proportional reduction of X-ray scattering intensity from the glassy phase as crystallization develops. Thick specimens (5 mm) of the parent glassy (pg), the glass–ceramic (gc = test specimens) and a mechanically mixed powder of pure crystalline species of the compound (gm), having the same chemical composition as the parent glass, were involved in the measurements. X-ray diffractograms were obtained for all the three samples and the peak intensity at a single angle 2θ was determined. The selection of 2θ was based on the broadest peak available for the parent glass. The percentage crystallinity (P_{CR}) in a particular specimen can then be expressed as:

$$P_{CR} = 100[(I_{pg} - I_{gc})/(I_{pg} - I_{gm})]$$

where I_{pg} is the X-ray intensity of parent glass, I_{gc} the X-ray intensity of test specimen and I_{gm} the X-ray intensity of mixture of crystalline species.

The pure crystalline, mechanically-mixed, powder was used to correct for background scattering effects (from air and the instrument). It was assumed that the absorption coefficient of the parent glass does not differ significantly from that of the residual glassy phase of the glass–ceramics. Crystallinity contents in the glass–ceramic specimens (based on three determinations of each) are summarized in Table III.

Bulk chemical analyses of the samples were obtained by an X-ray fluorescence technique. Full details of specimen preparation and analytical procedures are reported elsewhere [16]. The chemical composition is presented in Table IV.

TABLE II Density and grain size of glass–ceramics

Parameters	Specimens		
	GC 138.1	GC 138.2	GC 138.3
Bulk density ($g\,cm^{-3}$)	2.832	2.776	2.731
STD	0.003	0.003	0.004
Grain size (μm)	1.782	1.780	1.783
STD	0.609	0.607	0.615

STD = Standard deviation.

TABLE III Crystallinity content of the glass–ceramics

Specimen	% Crystallinity
GC 138.1	88.62 ± 1.17
GC 138.2	86.23 ± 1.65
GC 138.3	38.63 ± 1.48

3. Studies of electrical properties

3.1. Dielectric breakdown tests

The specimens for the breakdown test were prepared as 26 mm diameter discs, which were edge-rounded, diamond-ground and polished to mirror-like finish. Before use, they were washed in soapy water, then ethylene, dried and examined optically. Gold contacts were vapour deposited on each face (Fig. 1).

For the breakdown tests a hemispherically-ended electrode system was clamped to specimens (Fig. 1). The contact faces of the brass electrodes were of 8 mm diameter and highly polished. This type of electrode arrangement minimizes the risk of flash-over effects and reduces corona discharges [11].

In order to prevent flashover effects during operation the entire system was immersed in an oil bath. Immersion was slow to avoid bubble formation. The transformer oil employed was cleaned, degassed and dried prior to use.

Standard a.c. breakdown tests were performed at room temperature (18° C) and 50 Hz for 20 individual specimens of each type. In most cases a continuous steady-state voltage rise of $2\,kV\,sec^{-1}$ was applied to the specimens up to the breakdown point. Sufficient tests were performed to examine the effects of rate of voltage rise, surface finish (highly polished specimens), specimen thickness and crystallinity content on dielectric breakdown strength.

TABLE IV Typical composition of the glass–ceramics

Elements	Composition (wt %)	Standard deviation
Al_2O_3	30.67	0.25
SiO_2	45.18	0.26
MgO	12.62	0.08
TiO_2	11.72	0.09
Fe_2O_3	0.02	(0.01)
Cr_2O_3	0.01	–
Na_2O	Trace	–
CaO	Trace	–

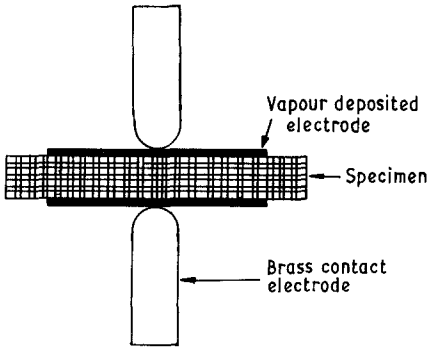

Figure 1 Arrangement for breakdown tests.

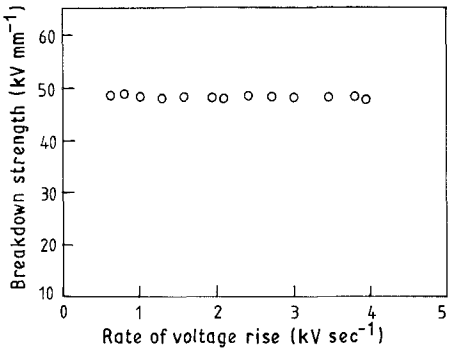

Figure 3 Variation of breakdown strength of glass-ceramic (GC 138.1) with rate of voltage rise.

3.2. A.c. resistivity and dielectric loss

The electrical resistivity and dielectric loss of GC 138.1 specimens were determined in air at temperatures of 18 to 800° C. The a.c. frequency range was 20 Hz to 300 kHz. A simple a.c. conductivity test cell was used [16] for the low and high temperature measurements. Before use the specimens were ground, polished down to 1μm diamond paste, washed in water and ethylene, then gold-coated, by sputtering (using appropriate masks), to provide the electrodes (Fig. 2). The basic three-probe technique was employed [20], for the plane-parallel specimens. The upper central electrode was of radius (r) 5 mm, the outer (guard-ring) electrode 6 mm wide and the gap (g) between the guard and central electrode was of the size required to meet the condition $g \leqslant 2d \leqslant r$ [20]. The lower electrode was of 9 mm radius. Suitable measurements were made with an a.c. bridge (Wayne Kerr 6425) in order to determine the resistivity and dissipation factor variations for the samples. These measurements were restricted to GC 138.1 specimens because of its high crystallinity content and breakdown strength. Whenever the temperature was changed the specimens were allowed to equilibrate for a minimum of 3 h in order to ensure thermal and parametric stability.

4. Results and discussion

The grain size data for the glass ceramics (Table II) indicate no significant differences between the sets of samples; but there is some variation in the density data (Table II). This implies that the crystallization process modified the bulk densities of the specimens. Furthermore there were uniform grain size distributions.

X-ray diffraction analysis showed that GC 138.1 glass–ceramic consisted mainly of crystalline β-cordierite with TiO_2 in the rutile phase. GC 138.2 contained similar crystalline phases but the TiO_2 in GC 138.2 was partially reduced but still in the rutile form. The glass-phase content of GC 138.2 was slightly higher than that of GC 138.1. In contrast, GC 138.3 glass ceramics consisted of β-quartz solid solution with the glass content well above 60%.

The microstructures of all the glass–ceramic specimens were broadly similar and comprised fine crystalline particles embedded in a continuous glassy matrix. The major differences between the specimens were in the crystallinity contents and the phases present.

As the three sets of glass–ceramics were obtained from the same parent glass, the bulk chemical compositions were the same. A typical analysis is shown in Table IV.

Using specimens of different type and thickness the effect of rate of voltage rise on breakdown strength was examined. Figure 3 shows that the breakdown strength was independent of the rate of voltage rise over a wide range of conditions. This observation is consistent with the behaviour expected for avalanche breakdown [6, 11, 13] which is an electronic process.

The variation of breakdown strength with specimen thickness for all samples is presented in Fig. 4. The data are based on at least 30 individual measurements for each sample at each thickness. Results for the variation of breakdown strength with surface finish (highly polished specimens), and crystallinity content are summarized in Tables V and VI.

The fact that the breakdown strength of the glass–

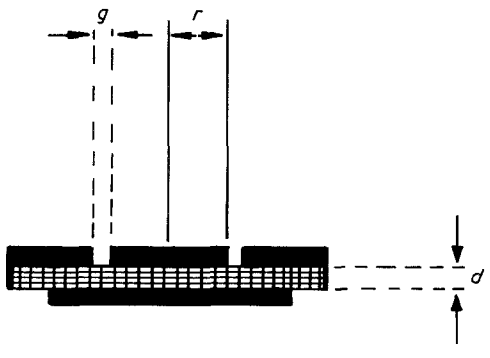

Figure 2 Specimen-electrode system for electrical conductivity measurements.

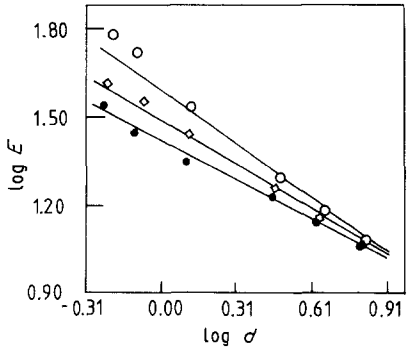

Figure 4 Effect of specimen thickness (d) on breakdown strength E (kV mm^{-1}) of glass–ceramics. (○) GC 138.1, (□) GC 138.2, (●) GC 138.3.

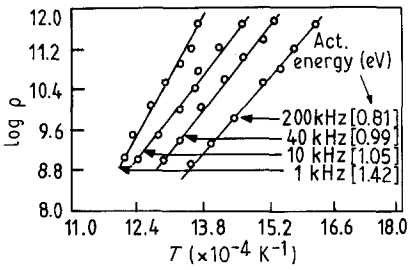

Figure 5 Variation of resistivity (Ωcm) with temperature and frequency for glass–ceramic GC 138.1.

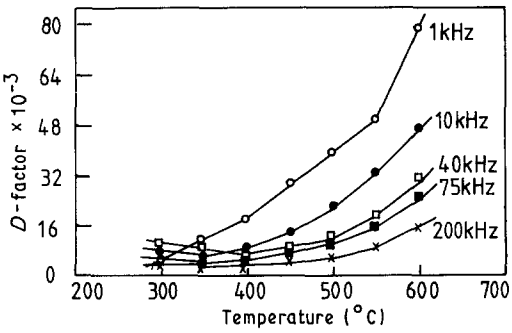

Figure 6 Variation of dissipation (D) factor with frequency and temperature for glass–ceramic GC 138.1.

ceramic was independent of the rate of voltage rise suggests an electronic process. It is believed that electrons were initially produced by a field emission process at the electrode–specimen interface. These electrons repeatedly bombard the surface of the material producing more electrons by secondary emission and collision processes. The net result was visible during the breakdown tests performed in the dark by multiple glow and minute sparks.

There was a significant increase in breakdown strength with improved surface finish and increased crystallinity content. Improved surface smoothness reduces the effect of local field concentrations and corona discharges on premature breakdown [21, 22]. Consequently, a more uniform field distribution leads to higher breakdown strengths. Similarly, an increased crystallinity content implies a reduction in the volume of glass-phase. The latter phase has a slightly higher electrical conductivity than the crystalline phase. Thus with increasing crystallinity content, a more homogeneous system is formed and this tends to result in higher breakdown strengths.

Fig. 4 demonstrates that the breakdown strength of the glass–ceramic specimens decreased exponentially with increasing specimen thickness. This is probably due to the higher chance of encountering breakdown initiating flaws (glassy phase, microcracks, bubbles and grain boundaries) within the effective volume (between the electrodes) as the specimen thickness increases. Regression analyses of the data yield the following expressions:

$$\text{GC 138.1:} \quad E = 46d^{-0.70}$$

$$\text{GC 138.2:} \quad E = 35d^{-0.66}$$

$$\text{GC 138.3:} \quad E = 30d^{-0.57}$$

Hence, generally, $E = Ad^{-n}$, where d is the specimen thickness and A and n are characteristic constants for the materials. These constants appear to reflect the dielectric quality of the specimens, which is dependent upon composition, density and the phases present. Furthermore, the decrease in breakdown strength with increasing thickness suggests that the major factor contributing to low breakdown strength is bulk defects (associated with the glassy phase) [23] rather than surface defects.

The electrical resistivity and the dissipation factor for glass–ceramics are shown as a function of temperature and frequency in Figs 5 and 6, respectively. As expected the resistivity decreases with increasing temperature whilst the dissipation factor increases with increasing temperature. However, the dissipation factor decreases with increasing frequency. Thus as the temperature of the system is increased the conductivity increases and any local increase in temperature causes further increase in the dissipation factor. Hence, the electrical resistivity and energy loss behaviour of the material will play a major role in the breakdown processes. At low frequencies and high temperatures the specimen will receive more energy than it loses and so the conductivity will increase. The accumulation of energy leads to high electrical losses and assists thermal breakdown processes.

5. Electron microscopy

Electron optic techniques (based on Philips 505 and 525 scanning electron microscopes) were used for microstructural and microchemical investigations of representative specimens after breakdown tests. These studies were performed in order to establish the breakdown mechanism. The breakdown process is characterized by an explosive sound and a sparking event. This results in the formation of an irregular breakdown channel which terminates in a crater at the surface of the specimen (Fig. 7a, b). The crater exhibits multiple cavities, surface tracking features, cracks and markings (solidification structures) (Figs 7b, 8 to 11). Cracks were randomly dispersed within the crater and surface tracking was pronounced (Figs 7b, 9, 11). The latter may have been caused by the relatively high electrical conductivity of the glass–ceramics.

The dominant morphology observed at the crater surface was well-defined spherical particulate

TABLE V Variation of breakdown strength with surface finish for glass–ceramics (GC 138.1) (high quality surface polishing)

Type of finish	Breakdown strength (kV mm^{-1})
As-received	26.4 ± 1.7
7 μm	29.5 ± 1.9
2 μm	41.5 ± 1.1
0.25 μm	65.4 ± 1.1

TABLE VI Variation of breakdown strength with crystallinity content for glass–ceramics (all specimens were polished to 1 μm for a short period)

Specimen	% Crystallinity	Breakdown strength (kV mm^{-1})
GC 138.1	89	31.7 ± 1.7
GC 138.2	86	27.1 ± 1.5
GC 138.3	39	19.4 ± 1.8

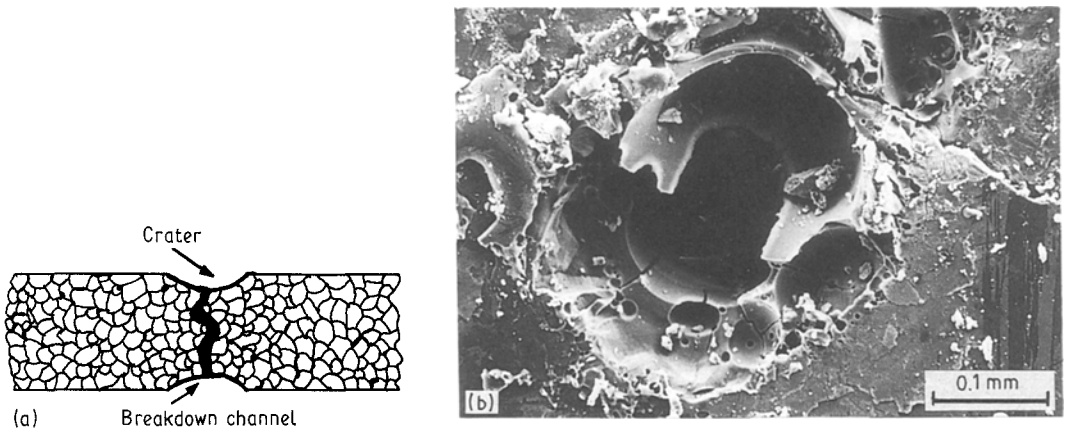

Figure 7 (a) Schematic diagram of breakdown channel and crater. (b) SEM micrograph of typical breakdown crater.

structures (Figs 10 and 11) which are thought to be solidification patterns. The multiple cavities found within the craters might have resulted from occluded gas or bubbles formed within the material during breakdown.

The breakdown channel (Figs 7a, 12), observed in fracture sections was smooth sided and irregular in shape. The smoothness of the channel wall suggests that some form of melting and liquid flow has occurred. It also indicates that the viscosity of glass–ceramic melt was relatively low. This characteristic of the breakdown channel might have been influenced by the amount of the glassy phase and its microstructure. Indeed channels in specimens of GC 138.3 were smoother than those in specimens of GC 138.1.

It is proposed that the crystalline structures observed at the crater surface resulted from an atomization process which followed breakdown. As the voltage is increased, breakdown is initiated leading to melting, the formation of a continuous breakdown channel and puncture. These processes cause vaporization and rapid cooling of the melt. Jones [24] reported that local melting with rapid ambient cooling could cause fragmentation of molten charges (i.e. an atomization process). Thus, it is possible that with voltage rise and breakdown channel formation, the molten charges which were previously within the channel were squeezed out on to the surface of the specimen in the oil bath. The accompanying explosive sound, forces and sparks could also assist the fragmentation of the molten charges as they reach the specimen surface. Once the melt flows to the surface, the relatively low ambient temperature (of the oil) should give rise to rapid cooling which will in turn enhance the solidification or crystallization of the material. It is not surprising that the breakdown channel is smooth since it cools at slower rate than the crater.

The results of chemical analysis performed at random locations within the crater regions are summarized in Table VII. The data indicate a random variation from point-to-point which differs from that of the bulk material. In general, Al_2O_3 and TiO_2 concentrations are lower within the crater region (including the solidification patterns) whilst SiO_2 and MgO concentrations are higher. Similar random variations in composition were also observed in the breakdown channels. These changes in concentrations may have been due, in part, to melting and vaporization of the material and preferential movements of materials.

The variation of composition in the crater, the observed cracks and the formation of the breakdown channel suggests that thermal and electrochemical processes were involved. The solidification patterns tend to support these proposals.

6. Conclusions

The a.c. breakdown of $MgO–Al_2O_3–SiO_2–TiO_2$ glass–ceramic is believed to occur through a combination of electronic, thermal and electromechanical processes. The mechanisms are inferred from the fracture patterns, presence of melt, solidification structures,

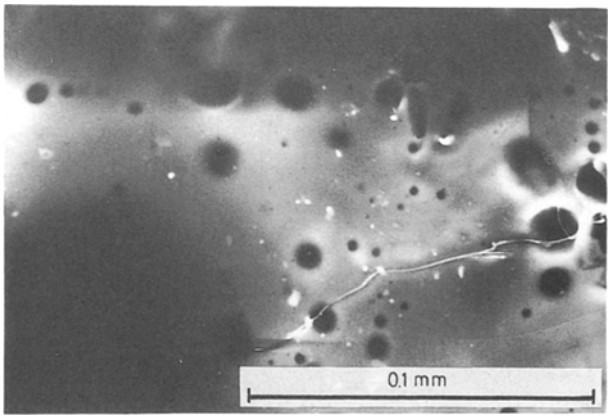

Figure 8 Detail of breakdown crater in specimen of GC 138.1 showing multiple cavities.

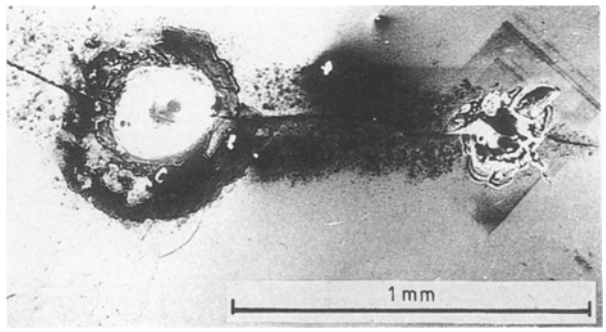

Figure 9 Surface tracking on glass ceramic GC 138.1.

Figure 10 Detail of crater in specimen of GC 138.1 showing spheroidal markings.

the formation of irregular breakdown channels, cracks and the fact that the breakdown strengths were independent of the rate of voltage rise, and decreased exponentially with specimen thickness.

Chemical analysis revealed a difference in composition between the crater regions (and breakdown channel) and the unaffected regions of the specimen. This suggests that a significant transfer of material occurred during the breakdown process.

A high percentage of crystallinity, good surface finish and homogeneous microsctructure yield high breakdown strengths, whilst poor microstructural development (characterized by low density, glass phase and lack of homogeneity) caused a significant reduction in breakdown strengths.

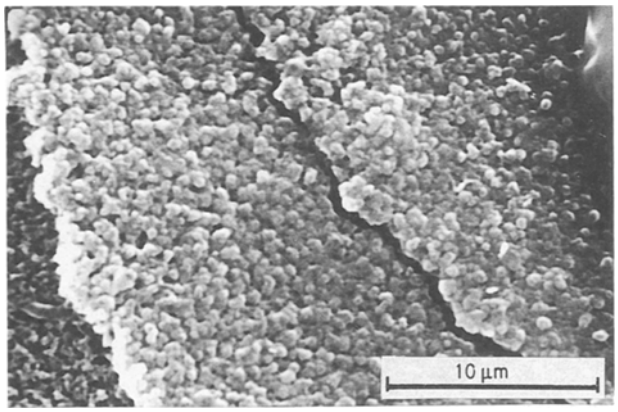

Figure 11 Solidification pattern in crater of specimen GC 138.1 after breakdown test.

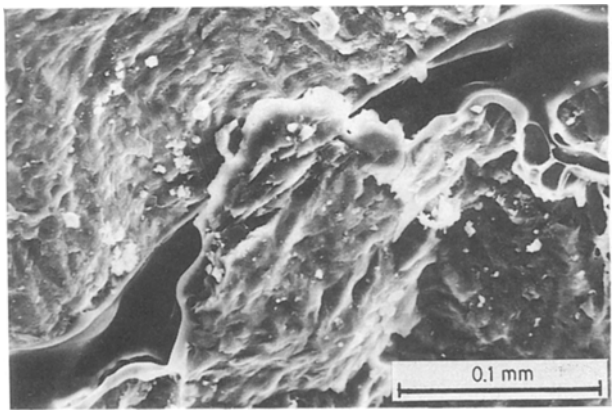

Figure 12 Fracture surface of specimen GC 138.2 showing breakdown channel.

TABLE VII EDAX analysis of major crater region of glass–ceramic at random locations

Specimen	Locations	Concentration (wt %) ± 0.1			
		Al_2O_3	SiO_2	MgO	TiO_2
		Original composition			
		30.6	45.2	12.6	11.7
GC 138.1	1	27.7	49.6	15.0	10.9
	2	27.1	49.6	16.9	12.4
	3	27.3	48.3	13.0	11.4
GC 138.2	1	24.7	52.6	14.6	9.3
	2	27.2	51.8	15.2	8.9
	3	20.0	54.6	14.9	5.8
GC 138.3	1	29.9	53.2	14.6	4.6
	2	26.2	51.0	12.8	12.1
	3	26.2	52.6	14.3	10.2

Acknowledgement

The authors wish to express their thanks and gratitude to Pilkington Brothers Ltd for provision of materials, and to Dr I. D. Couper and Mr D. A. Greaves (Department of Electrical and Electronic Engineering, UMIST) for access to the high voltage facilities and helpful discussions.

References

1. R. MORRELL, "Handbook of Properties of Technical and Engineering Ceramics", Part I, (National Physical Laboratory, UK, 1985), p. 121.
2. W. N. LAWLESS, *Cryogenics* May (1975) 273.
3. M. G. GEE, *Metals Mater.* Dec. (1986) 769.
4. L. A. LAY, *ibid.* May (1987) 250.
5. D. B. BINNS, *Proc. Brit. Ceram. Soc.* **18** (1970) 17.
6. S. HAYAKAWA, *Indust. Res. Devel.* **25** (1983) 146.
7. E. M. BALDWIN, E. P. HYATT and R. C. VICKERY, *IEEE Trans. Mater. Pack.* **PMP-1** (1965) 264.
8. T. NITTA, *J. Ceram. Soc. Jpn* **15** (1980) 346.
9. T. NITTA, T. TERADA and S. HAYAKAWA, *J. Amer. Ceram. Soc.* **63** (1980) 295.
10. R. W. SILLARS, "Electrical Insulating Material and Applications' (Institution of Electrical Engineers, 1973) p. 61.
11. R. BARTNIKAS, *Engng Dielectrics* (*ASTM*) **IIB** (1987) 157.
12. D. G. GROSSMAN, *Advan. Ceram.* **4** (1982) 249.
13. I. O. OWATE and R. FREER, *Sci. Ceram.* **14** (1988) 1013.
14. ASTM C373, Standard Test Method for Water Absorption, Bulk Density, Apparent Porosity and Apparent Specific Gravity of Fired Whiteware Products (1982).
15. G. F. VANDER-VORT, Symposium Proceedings on Practical Applications of Quantitative Metallography, edited by J. I. McCall and J. H. Steel (ASTM, 1984) p. 85.

16. I. O. OWATE, PhD Thesis, University of Manchester (1989).
17. Z. STRAND, "Glass Ceramics Materials" (Elsevier, New York, 1986) p. 158.
18. S. C. NYBURG, *Brit. J. Appl. Phys.* **5** (1954) 321.
19. S. M. OHLBERG and D. W. STRICKLER, *J. Amer. Ceram. Soc.* **45** (1962) 170.
20. N. M. TALLEN, "Electrical Conductivity in Ceramics and Glasses", Part A (Marcel Dekker, New York, 1974) p. 104.
21. Y. QIU, *IEEE Trans. Elec. Insul.* **E1-21** (1986) 673.
22. I. W. McALLISTER, *ibid.* **E1-21** (1986) 659.
23. Y. INUISH and D. A. POWERS, *J. Appl. Phys.* **28** (1957) 1017.
24. H. JONES, "Rapid Solidification", Monograph 8 (Institute of Metals, London, 1982) pp. 8–46.

Received 6 July
and accepted 12 December 1989